21st Australasian Fluid Mechanics Conference
Adelaide, Australia
10-13 December 2018

A Taylor-Couette System for the Experimental Study of the Influence of Surface Roughness

C. Atkinson[1], **S. Amjad**[1] **and J. Soria**[1,2]

[1]Laboratory for Turbulence Research in Aerospace and Combustion,
Department of Mechanical and Aerospace Engineering,
Monash University, Victoria 3800, Australia
[2]Department of Aeronautical Engineering, King Abdulaziz University,
Jeddah, Kingdom of Saudi Arabia

Abstract

An optically accessible Taylor-Couette flow has been setup to enable experimental investigation of the influence of surface finish and roughness on the transfer of momentum between the wall and the bulk flow. Details of this facility and flow characterisation are presented, demonstrating the ability to explore flow regimes from laminar Taylor vortices to featureless turbulence.

Introduction

Naturally occurring or engineered surface roughness (riblets, superhyrophobic surfaces) can have a significant effect on wall-bounded flows. Despite the tendency for the surfaces of many rotating flow system such as bearings, compressor and turbines to develop roughness due to wear and pitting, relatively little is known about how such roughness influences the structure of the boundary layers in these flows and how this affects the interaction with the bulk flow. In the more general case of streamwise developing boundary layers and finite length channel flows over rough surfaces, it is difficult to assess the extent to which the flow structure is a function of the local conditions (e.g. local surface roughness, temperature) and the degree to which it depends on the upstream evolution and history of the flow. One method of decoupling these effects is to study the flow in a self-similar state, such that the relative contribution of each term in the governing equations is independent of streamwise position. In the case of surface roughness such a state can potentially be achieved by considering a flow that is streamwise periodic and hence independent of streamwise position. While the later is readily done in direct numerical simulations of pipes and channels, obtaining the equivalent flow in an experimental facility is often hampered by limited streamwise extent.

One practical flow that avoids streamwise dependence, is the flow between two-coaxial independent rotating cylinders, Taylor-Couette flow. This configuration results in a statistically homogeneous flow in the azimuthal direction once a statistical stationary state has been reached. Taylor-Couette flows exhibit significant variations in the nature of the flow depending on the Taylor number and the Reynolds numbers of the inner and outer cylinders, which both represent the ratio of rotational inertial force to viscous forces. In the case of a rotating inner cylinder and a stationary outer cylinder the definition of the Taylor, Ta, and Reynolds number, Re_i, reduce to:

$$\mathrm{Re}_i = \frac{r_i \omega_i (r_o - r_i)}{\nu} \quad (1)$$

$$\mathrm{Ta} = \frac{(1+\eta)^4}{64\eta^2} \frac{(r_o - r_i)^2 (r_i + r_o)^2 \omega_i^2}{\nu^2} \quad (2)$$

where r_i and r_o are the radii of the inner and outer cylinders, ω_i is the rotational speed of the inner cylinder, ν is the kinematic viscosity of the fluid and $\eta = r_i/r_o$. In the case of smooth inner and outer walls the flow regimes vary from laminar Couette flow, to turbulent Taylor vortices with laminar boundary layers, through to a featureless turbulence with turbulent boundary layers on both walls [4]. Surface roughness will modify the boundary layers and is therefore expected to modify the interaction between the boundaries and the bulk flow and the transfer of momentum from the inner wall to the flow.

Cadot *et al.* [2] performed experiments on a Taylor-Couette flow, with $\eta = 0.625$, $\mathrm{Re}_i = 1 \times 10^4$ to 3×10^5 consistent with featureless turbulence, for a smooth rotating inner and smooth stationary outer wall, and after adding axially aligned ribs on both the inner and outer cylinders acting as roughness with a height of $0.067d$. At these conditions the addition of the riblets was found to increase the required driving torque and reduced the sensitivity to Reynolds number seen in the absence of the riblets, resulting in a flow where energy dissipation is dominated by the bulk flow. Changes in velocity profiles and structure of the flow were not captured. Van den Berg *et al.* [1] also studied the influence of rough walls on the torque required to drive a Taylor-Couette flow with $\eta = 0.73$, $\mathrm{Re}_i = 1 \times 10^4$ to 1×10^6, considering cases where both walls are rough and when one of the two walls remains smooth. Again, the roughness took the form of square riblets aligned in the axial direction. Results showed that keeping at least one surface smooth preserved the Reynolds number dependence while the addition of each rough wall increased the relative contribution of the bulk flow to the total energy dissipated by the flow.

Recently, Zhu *et al.* [7] performed direct numerical simulations to analyse the source of the greater energy dissipation for rough wall Taylor-Couette flows, with $\eta = 0.714$, $\mathrm{Re}_i = 8 \times 10^3$ to 8×10^4. Roughness again took the form of axially aligned square rods with height $0.1d$, this time only on the inner rotating cylinder. Simulations showed that the increase in torque at the wall was due to the pressure drag associated with the roughness elements, with the increase in bulk dissipation being due to the vortices shed from the roughness elements that are then transported to the bulk flow by the Taylor vortices.

In this paper we discuss the design and characterisation of a Taylor-Couette facility with a driven inner cylinder for the experimental investigation of the influence of different natural and engineered roughness and surface coatings on the energy dissipation, required driving torque, and flow structure.

Taylor-Couette System

To assess the influence of different surface roughness and coatings on the resulting flow structure an optically accessible Taylor-Couette system with a transparent acrylic stationary outer cylinder was established with the geometry summarised in table 1. The outer cylinder is housed within a water filled clear rectangular acrylic tank in order to reduce the influence of the changes in refractive index and the optical distortions that are created when imaging through the cylindrical surface (see figure 1). Both the top and bottom end caps of the cylinder

Inner radius	r_i	80	mm
Outer radius	r_o	95	mm
Radius ratio	η	0.842	
Gap size	d	15	mm
Length	L	1.2	m
Kinematic viscosity	ν	9.562×10^{-7}	m^2/s

Table 1: Taylor-Couette system and flow parameters.

are fully submerged in water with a flooded 1 mm gap between the cylinder end surfaces and those of the outer tank. The inner cylinder is driven by a rs43C Compumotor stepper motor driven by a JMC 2DM2280 motor driver with step timing provided by an in-house timing unit developed using an Beaglebone black board computer [3]. For the present measurements the motor was run with 1600 steps per revolution and accelerated exponentially from rest, asymptoting to a target inner cylinder rotation rate in two minutes for each case. An inline torque transducer is placed between the motor and the cylinder to directly measure the torque required to drive the inner cylinder. In this configuration the inner cylinder is able to achieve a rotational rate of up to 300 revolutions per minute (rpm). Beyond this the imperfect balance of the cylinder and the high centre of gravity associated with the top mounted motor, results in noticeable vibration of the facility. Alterations are being made to the setup to enable in-situ adjustment and balancing of the inner cylinders with different surface finishes and to enable the higher rotation rates needed to achieve truly featureless turbulence [4].

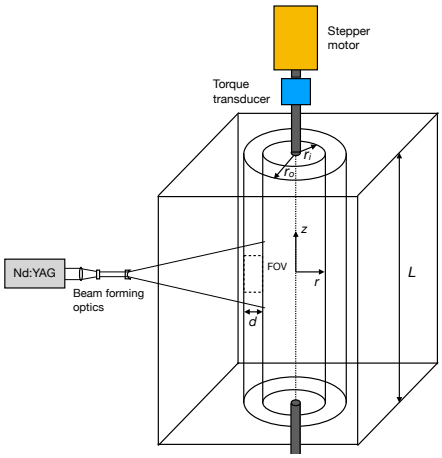

Figure 1: Schematic of Taylor-Couette system and particle image velocimetry configuration.

Velocity field measurements

Planar particle image velocimetry (PIV) measurements are performed to investigate the radial and axial components, $\tilde{u}_r$ and $\tilde{u}_z$, of the instantaneous fluid velocity in the $r-z$ plane. The annular flow consisted of distilled water seeded with nominally 11 μm diameter Potters hollow glass spheres with a specific gravity of $\gamma = 1.1$. Iodised salt was added to increase the salinity of the solution to 100 ppm to prevent the build up of static charge on the acrylic outer cylinder that might otherwise interfere with the seeding particles. Illumination was provided by a dual cavity 300 mJ Quantel Brillant B Nd:YAG laser with a series of cylindrical lenses used to form a collimated, approximately 1 mm thick light sheet. Particle images were recorded using a double shutter PCO.4000 CCD array camera coupled with a $f = 200$ mm Micro Nikkor lens at a rate of 2 Hz. The aperture of the lens was closed down to $f_\# = 22$ in order to reduce the distortions of the particle images associated with the wall curvature. Fortunately, the laser energy was more than sufficient to ensure high contrast particle images, however the large particle image diameter and out of plane motions required the used of a larger interrogation window. Details of these PIV and image parameters are provided in table 2.

Magnification	$M = 0.829$	
Spatial resolution	92.1	pixels/mm
Lens focal length	$f = 200$	mm
Lens aperture	$f_\# = 22$	
Particle diameter	$d_p = 11$	μm
Particle image diameter	$d_{pi} = 5.9$	pixels
Diffraction limited depth of field	$dof = 6.12$	mm
Light sheet thickness	$\Delta_z = 1$	mm
Interrogation window size	128, 128 (first pass)	pixels
	64, 64 (final pass)	pixels
Vector spacing	16, 16 (final pass)	pixels

Table 2: Particle image velocimetry parameters.

A series of different rotational speeds where chosen to cover what was expected to span the gamut of flow regimes from laminar to turbulent Taylor vortices to the verge of a featureless turbulent bulk flow. The rotational rate and corresponding Re_i and Ta for each case are detailed in table 3. The interframe time between each particle image was varied from 0.16 to 20 ms in order to reduce the out of plane particle motion. The out of plane motion was adjusted to approximately 40% of the light sheet thickness in all cases. This limits the in-plane displacement to around 6 pixels and restricts the dynamic range of measurements in the $r-z$ plane. The lights sheets from the two cavities could be offset to reduce the out of plane motion of the bulk flow and hence enable larger in-plane displacements, however this would required a realignment of the light sheets for each measurements speed and hence is only viable once a particular target speed has been identified.

rpm	Δ_t (ms)	$r_i\omega_i$ (mm/s)	Re_i	Ta
1.5	20	12.6	1.93×10^2	4.50×10^4
5.0	10	41.9	6.42×10^2	5.00×10^5
10.0	5.0	83.8	1.28×10^3	2.00×10^6
20.0	3.0	168	2.57×10^3	8.00×10^6
50.0	1.0	419	6.42×10^3	5.00×10^7
100	0.46	838	1.28×10^4	2.00×10^8
300	0.16	2513	3.85×10^4	1.80×10^9

Table 3: Inner cylinder rotational rate and corresponding Reynolds and Taylor number for present measurements.

Particle images were processed using an in-house multi-grid [5] digital cross-correlation PIV code, combined with a three pass normalised median vector validation [6]. A secondary validation was then applied based on the local histogram of the velocity at each point in the flow across the measurement ensemble.

Results

A series of 600 velocity fields were recorded for each of the inner cylinder speeds listed in table 3. Figure 2 shows the mean vector fields (every 3rd vector shown) and contours of the mean velocity magnitude. In all cases we observe the presence of Taylor vortex cells, with the lowest Taylor number considered expected to be the point at which these structures begin to form in the bulk flow. The present field of view was sufficient to capture about one and a half of these structures. The mean structure

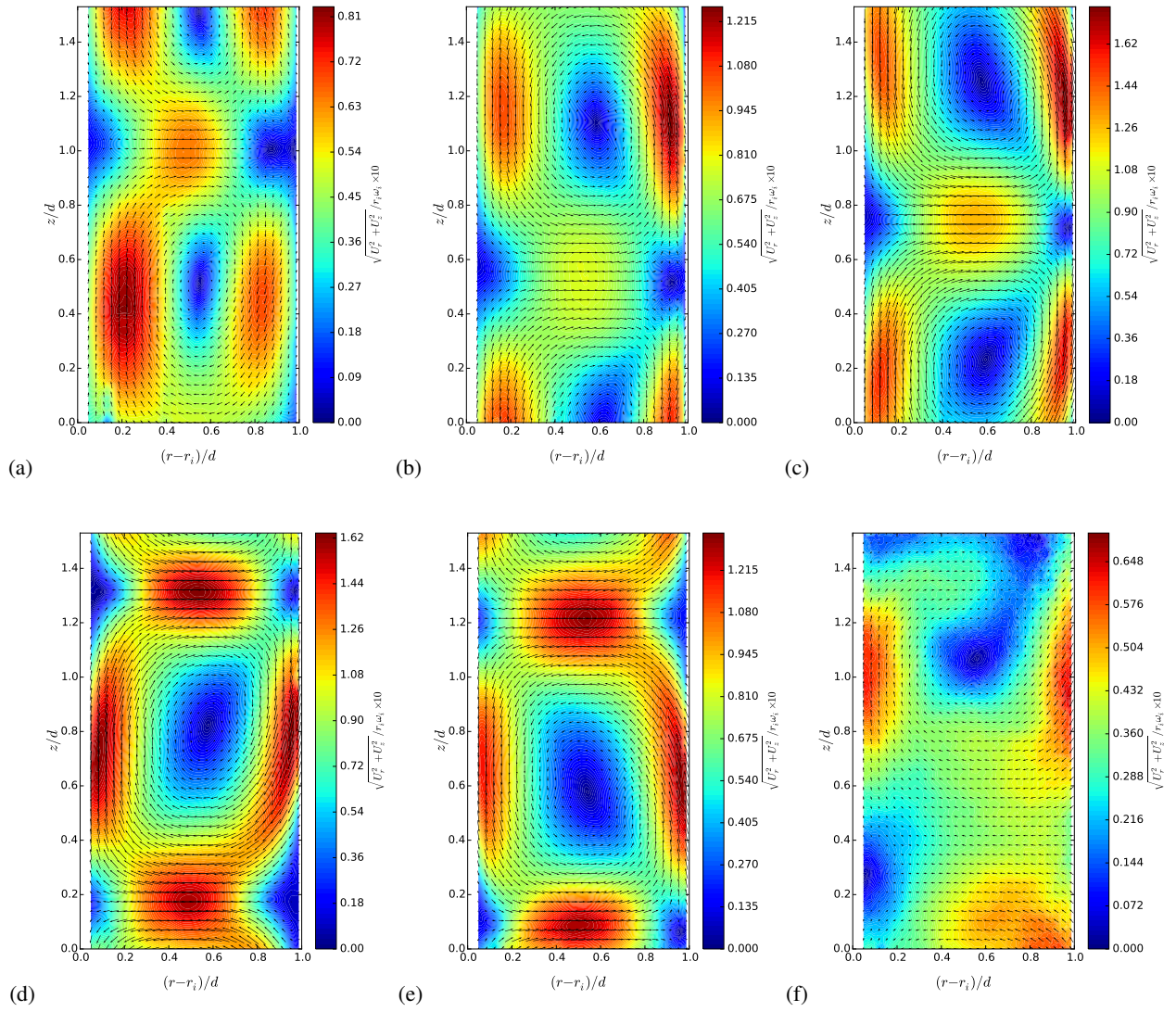

Figure 2: Ensemble mean vector fields (every third vector shown) and iso-contours of the mean velocity magnitude in the $r-z$ plane for Taylor numbers: (a) 4.50×10^4; (b) 2.00×10^6; (c) 8.00×10^6; (d) 5.00×10^7; (e) 2.00×10^8 and (f) 1.80×10^9. Velocities are normalised by the azimuthal velocity at the surface of the inner cylinder for each case, $r_i\omega_i$.

of this flow remains fairly consistent from a Taylor number of 10^4 to 10^8. The magnitude of the in-plane velocity increases relative to the azimuthal speed of the cylinder up to Ta = 10^7, after which the relative velocity in the Taylor vortices begin to diminish as a state of featureless turbulence is approached.

Figure 3 shows the contribution to the fluctuating kinetic energy from fluctuations in the u_r and u_z velocity components. This represents all fluctuations from the mean flow at a fixed location relative to the stationary outer cylinder and therefore includes both the contribution from the relative movement of the Taylor vortices with respect to both time and the position of the inner cylinder, as well as any contribution from turbulent velocity fluctuations. Without measurements of the azimuthal velocity fluctuations it would be unreasonable to comment on any apparent increase in the fluctuating kinetic energy, however changes can be observed in the locations of the peak fluctuations for the different flow cases. For the lower Taylor numbers, the largest fluctuations occur near the inner and outer walls, in-between the Taylor vortices, where the mean in-plane velocity is at a minimum. These regions become more tightly focused and move closer to the walls with higher rotation rates as the in-plane velocity increases with respect to the bulk azimuthal velocity, until Ta $= 10^7$ where rotation in the mean velocity field begins to decrease. At this point the strongest fluctuations shift away from the wall towards the centre of the gap and the interface between the the Taylor vortices, until Ta $= 10^8$. At Ta $= 10^9$ the peak fluctuations are again located near the walls, however fluctuations are also starting to appear in the core of the Taylor vortices. Results suggest that a further increase in the rotation rate should be sufficient to reach a state of featureless turbulence, however this will require balancing of the rig and the isolation of structural vibrations.

Conclusions

An experimental facility has been developed that will allow the investigation of the influence of surface roughness and finishes on the structure of a Taylor-Couette flow using laser diagnostic velocimetry techniques. The current facility is cable of exploring flows from the initial appearance of laminar Taylor vortices to the verge of a featureless turbulent state. Additional cylin-

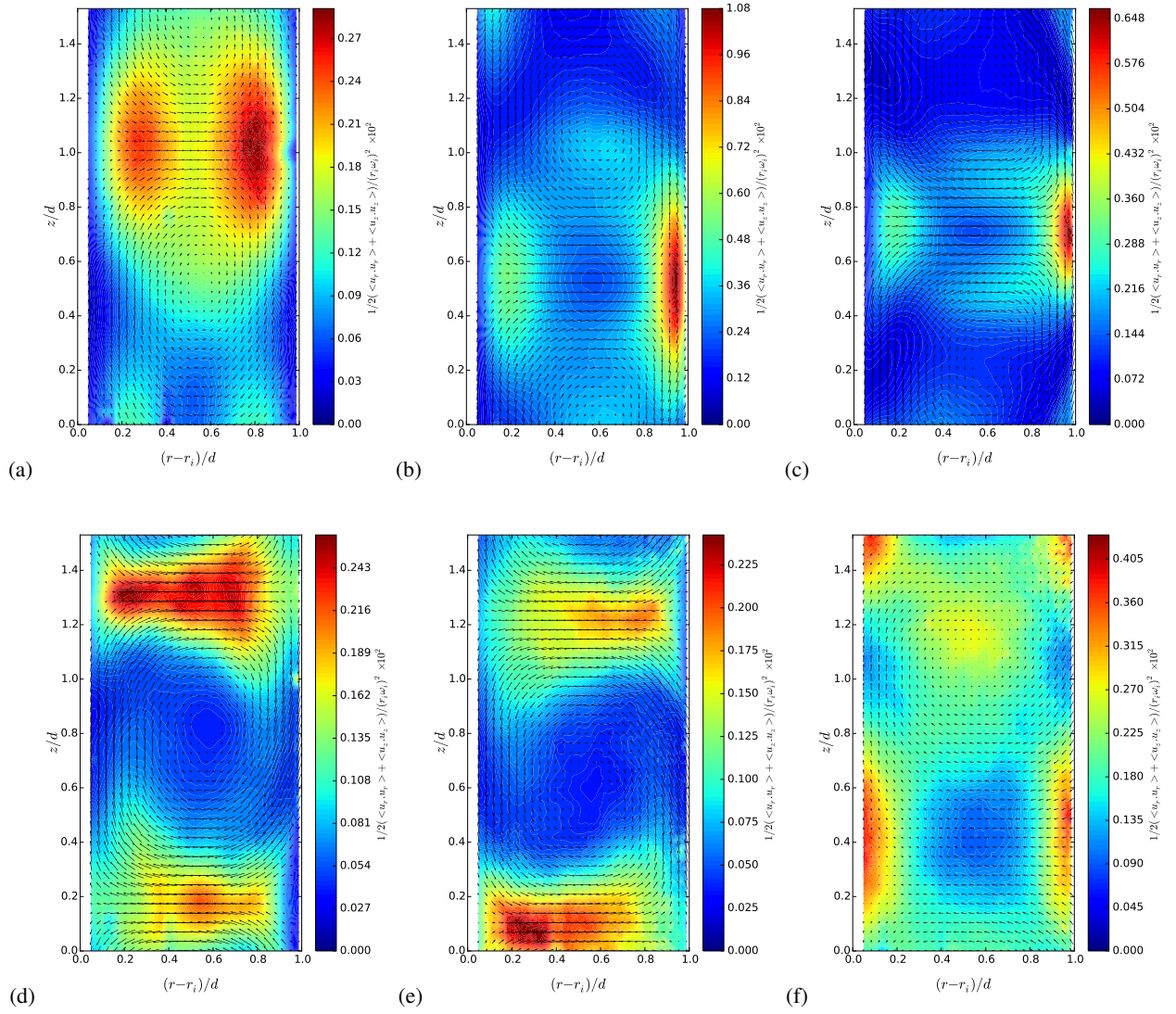

Figure 3: Ensemble mean vector fields (every third vector shown) and iso-contours of the fluctuating kinetic energy associated with the fluctuations in the radial and axial velocity components i.e. $1/2(u_r^2+u_z^2)$ in the $r-z$ plane for Taylor numbers: (a) 4.50×10^4; (b) 2.00×10^6; (c) 8.00×10^6; (d) 5.00×10^7; (e) 2.00×10^8 and (f) 1.80×10^9.

ders are currently being prepared for the application of different surfaces finishes.

Acknowledgements

The authors would like to acknowledge the research funding from the Australian Government through the Australian Research Council (ARC). Dr. Atkinson was support by an ARC Discovery Early Career Research Award fellowship while undertaking this work.

References

[1] van den Berg, T.H., Doering, C.R., Lohse D., and Lathrop, D.P., Smooth and rough boundaries in turbulent Taylor-Couette flow, *Phys. Rev. E*, **68**, 2003, 036307-1–5.

[2] Cadot, O., Couder, Y., Daerr, A., Douady, S. and Tsinober, A., Energy injection in closed turbulent flows: Stirring through boundary layers versus inertial stirring, *Phys. Rev. E*, **56**, 1997, 427–433.

[3] Fedrizzi, M., and Soria, J. (2015). Application of a single-board computer as a low-cost pulse generator. *Measurement Science and Technology*, **26**(9), 095302.

[4] Grossmann, S., Lohse, D. and Sun C., High-Reynolds Number Taylor-Couette Turbulence, *Ann. Rev. Fluid Mech.*, **48**, 2016, 53–80.

[5] Soria, J. An investigation of the near wake of a circular cylinder using a video-based digital cross-correlation particle image velocimetry technique. *Exp. Thermal Fluid Sci.*, **12**, 1996, 221233.

[6] Westerweel, J., and Scarano, F., Universal outlier detection for PIV data, *Exp. in Fluids*, **39**, 2005, 1096?1100.

[7] Zhu, X., Verzicco, R., and Lohse D., Disentangling the origins of torque enhancement through wall roughness in Taylor-Couette turbulence, *J. Fluid Mech.*, **812**, 2017, 279-293.